Toward Faithfulness-guided Ensemble Interpretation of Neural Network

Siyu Zhang[1] and Kenneth Mcmillan[2]

[1] University of Texas at Austin, Austin TX 78701, USA zhangsiyu@utexas.edu
[2] kenmcm@cs.utexas.edu

Abstract. Interpretable and faithful explanations for specific neural inferences are crucial for understanding and evaluating model behavior. Our work introduces **F**aithfulness-guided **E**nsemble **I**nterpretation (**FEI**), an innovative framework that enhances the breadth and effectiveness of faithfulness, advancing interpretability by providing superior visualization. Through an analysis of existing evaluation benchmarks, **FEI** employs a smooth approximation to elevate quantitative faithfulness scores. Diverse variations of **FEI** target enhanced faithfulness in hidden layer encodings, expanding interpretability. Additionally, we propose a novel qualitative metric that assesses hidden layer faithfulness. In extensive experiments, **FEI** surpasses existing methods, demonstrating substantial advances in qualitative visualization and quantitative faithfulness scores. Our research establishes a comprehensive framework for elevating faithfulness in neural network explanations, emphasizing both breadth and precision

1 Introduction

The complex structure and high-dimensional embedding of state-of-the-art neural networks render them essentially uninterpretable to humans. This presents a significant barrier to comprehending their internal functioning. It has been established that a good explanation should satisfy two criteria: faithfulness and interpretability [12,21]. Faithfulness measures the extent to which the explanation accounts for the reasoning process of the model, while interpretability emphasizes the degree to which the explanation is comprehensible to humans. These two criteria are mutually exclusive and can be evaluated separately. Much of the recent research on explaining neural networks focuses on generating attribution maps for input images [4, 25, 28],as these maps offer substantial interpretability with their visualizations.. An attribution map consists of importance values that quantitatively measure the causal relationship with the neural network output for a particular input. In other words, it assigns a heatmap to the input based on its relevance to model inference.

Evaluating attribution presents challenges since there is no universal agreement on objective metrics for assessing the quality of explanations. Interpretability of explanation is often evaluated qualitatively through visualization or quantitatively through human rating scores [18,21]. However, measuring improvements

in interpretability is challenging because it often involves human subjects. Consequently, researchers have shifted their focus to enhancing faithfulness. A new category of explanation methods has emerged, driven by faithfulness evaluation. These methods observe the network's output with perturbed input, typically investigating changes in the output when specific input features are removed. The underlying intuition behind these techniques is that explanation in the form of attribution map is faithful if highly-attributed features alone can produce output similar to the full input. Nevertheless, existing methods [7, 30] depend on a coarse approximation of faithfulness metrics as their objectives. This approach demands significant effort in hyperparameter tuning and still yields suboptimal results. Thus, a better objective is required for improve overall faithfulness.

Moreover, prior research often overlook the intermediate layers of neural networks when assessing faithfulness. While neural networks are frequently perceived as black-box models, they can be regarded as white-box models because every computation they perform and every value they compute in the model are visible. However, what renders these models intrinsically uninterpretable is the sheer magnitude of these variables, often numbering in the millions or even billions, making them impossible for human to comprehend. The white-box nature of neural networks implies that the model's reasoning process is encoded in the intermediate part of the model. Since faithfulness requires that the explanation accurately reflects the model's reasoning process, it is reasonable to assert that faithfulness measurements should encompass the hidden part of the model. In this paper, we focus on addressing the aforementioned challenges of both overall and internal faithfulness.

First, we introduce a novel ensemble method that closely aligns with perturbation metrics. Instead of optimizing a single attribution map, this approach formulates a superior approximation by optimizing multiple attributions, thereby achieving greater similarity with the actual evaluation metrics. Additionally, through the use of the ensemble method, we are able to eliminate the need for hyperparameters. Further details can be found in Secs. 3.1 and 3.2.

Furthermore, we achieve internal faithfulness by implementing gradient clipping techniques within the hidden layers. We choose gradient clipping due to its lightweight nature and the absence of additional gradient introductions. Additionally, working with gradients from perturbation optimization helps maintain overall faithfulness. We provide implicit evidence of the effectiveness of our technique in preserving faithfulness within the hidden layers through qualitative measurements via visualization, as demonstrated in Sec. 4.3. Our regulation method also prevents the emergence of adversarial noise during optimization, resulting in interpretable visualizations and improved quantitative faithfulness scores.

In this work, our primary focus lies within the domain of computer vision. However, we firmly believe that our method can be extended to other domains. In the evaluation section, we demonstrate the superiority of our techniques by achieving higher scores in quantitative faithfulness evaluations and by providing accurate and interpretable visualizations.

2 Background

2.1 Explanation genre

There is a wide range of prior work focused on explanation, mainly feature attribution.

Backpropagation-based Methods These methods calculate importance scores for input images by back-propagating information to the input . Such approaches are efficient as they typically require only a single forward and backward pass. For instance, Yan *et al*. [23] generate a saliency map based on ordinary gradients, while other works [25,26,30,32] regulate the gradient to reduce noise. Alternatively, some methods propagate different measurements based on gradients or activation to the input layer, as seen in works by [2,22,28], While these attribution maps are typically fine-grained, they can be challenging to interpret.

Activation-based Methods Activation-based methods aggregate the values of a specific layer to create a heatmap for input images [4, 21, 34]. While these visualizations are generally at a coarse level, they can be combined with back-propagation methods such as those by Springenberg *et al*. [26] to produce fine-grained visualizations at the input. However, it's important to note that these approaches can sometimes yield unfaithful results, as demonstrated by Adebayo *et al*. [1].

Surrogate Methods Another approach to explaining neural network decisions is to create a simple and interpretable surrogate model based on input and output examples. For instance, distillation [10] derives a shallow network from a deep network. LIME [18] , on the other hand, creates a linearized approximation of the target network's behavior around a given input image.

Perturbation-based Methods Perturbation-based methods revolve around the concept of perturbing individual inputs or neurons and examining the network's output. Some approaches, such as those by Petsiuk *et al*. [17] and Sun *et al*. [27], involve masking parts of images to calculate importance scores based on changes in model output. These methods vary in their techniques for occlusion and the heuristics used for ranking image features. Another category of perturbation-based methods focuses on optimization, seeking to find a mask that has the maximum or minimum impact on the model's output [6,7,30]. However, the optimization process often introduces adversarial noise, necessitating various regulation methods such as mask smoothing [6], gradient clipping [30] and resolution reduction [7]. While these methods are typically faithful to the model's predictions by design, they can be relatively computationally inefficient. Our method falls into this category. By defining a more appropriate objective and promoting internal faithfulness, our method enhances evaluation scores while simultaneously improving efficiency.

2.2 Evaluation for explanation

Different evaluation mechanisms for explanations have been proposed to assess their quality. Most of these mechanisms can be divided into two categories: Interpretability and Faithfulness.

Intepretability evaluation often requires explicit or implicit human judgment of the explanation. Experiments are conducted by hiring users to rate the quality based on its interpretability, as seen in previous studies [16] or its effectiveness in aiding specific tasks, as demonstrated by Ribeiro *et al*. [18]. Interpretability can also be quantitatively measured with implicit human judgment using methods such as the pointing game [33], which assesses the quality of the explanation by evaluating its alignment with a human-annotated segmentation map.

Faithfulness evaluation often involves measuring the relationship between the explanation and the model. One prevalent faithfulness test is the sanity test [1], which evaluates faithfulness to the model by comparing the change in visualization with parts of the model weight randomized. Another widely used metrics are the MoRF and LeRF tests proposed by Samek *et al*. [20], also known as the deletion and preservation tests. In essence, the deletion test posits that the removal of pixel information, starting from the most to the least salient pixels, should lead to a rapid decrease in the model output. On the contrary, preservation test remove pixel from the least to the most salient, resulting in a slow decrease in the category output. The test results can be quantitatively measured by plotting the curve of model output versus the deleted/preserved area fractile and computing the Area Under Curve(AUC) [3]. Some variations of this metric have been proposed. While most variations introduce changes in the perturbation [13], the remove-and-retrain metrics measure the change in model accuracy when retrained with perturbed data [11]. Our method is guided by analysis of existing faithfulness evaluation metrics while expanding faithfulness to the internal structure of neural networks.

3 Method

This work focus on explaining the task of image classification with attribution maps as explanations format as it is more intuitive to evaluate their performance both in interpretability and faithfulness. As mentioned, our work is driven by analysis of faithfulness evaluation, therefore lies in the genre of perturbation-based method. We begin by establishing a clear definition of faithfulness.

3.1 Faithfulness Metrics

Intuitively, an explanation is deemed faithful when it reliably aligns with the model. Specifically, in the context of an attribution map, we aim for the attribution values of features to accurately reflect the model's attention. In other words, for a given input, features with a higher attribution values possess a higher influence on the model output. By influence, we mean a tendency to reinforce the probability of the predicted category. One way to evaluate the influence of an input feature involves masking it in some manner and observing the resultant effect on the output. When masking a highly salient feature, we expect a reduction in the category output, whereas masking a feature of lower salience should

generally preserve it. However, when we consider a feature to be a single pixel, masking it often fails to have a meaningful impact on the category output. Thus, we must shift our focus towards assessing the influence of *ensembles* of pixels. Moreover, due to structure of images, the ensemble need to effective such that it contains meaningful information instead of purely noise.

To formalize this notion, we introduce a perturbation operator $\otimes$. Given an input value x (typically an image) and an ensemble of input features S, $x \otimes S$ yields a perturbed input value. This perturbation is usually achieved by masking the features within the ensemble S. We consider perturbation operators that mask pixels by replacing them either with a fixed background value or with a random value. Define $R = (x \otimes P)$ as a fully masked reference image, where P is the ensemble of all pixels. Let ϕ be the function that yields the predicted category output of a neural network on input x. We define the *influence* of ensemble S as $I(S) = \phi(x \otimes S) - \phi(x)$, that is, the difference in the estimated category probability resulting from masking the features within the ensemble S.

The influence of a single pixel can then be defined as the sum of the influence of all effective ensembles it belongs to. Formally, given a single pixel $p \in P$, the *influence* of p can be defined as

$$I(p) = \sum_{p \in S, S \in E} I(S) \tag{1}$$

where E is a set of effective ensembles e such that $e \subseteq P$. Deciding the ensembles can be a tricky question. A naive way of solving the problem is to use image segmentation to preprocess the input into several ensembles [18]. However, such methods enforce a strong prior on the explanation such that model perception of input is similar to the segmentation map, which has not been proved.

The challenge of identifying effective ensembles, coupled with the computational resources required for Eq. (1), renders it impractical to directly compute the influence of every pixel. However, since the goal is to to assess the faithfulness of an existing attribution map, effective ensembles can be approximated. For this purpose, Binder *et al.* [3] propose to consider the *fractiles* of attribution map. Intuitively, the explanation given by attribution map is interpreted as relevant and irrelevant features of the model decision, which can be captured by the *upper* and *lower* fractiles of the attribution map. Formally, Suppose we are given an attribution map M, which assigns real numbers to features indicating their salience. Given a fraction $f \in [0, 1]$, the *upper* f-fractile is defined as the set of pixels with saliency values greater than a fraction f of all the pixels. Conversely, the *lower* f-fractile consists of pixels with saliency values *less* than a fraction f of all the pixels. If the attribution is faithful, the upper fractiles should exhibit relatively high influence, while the lower fractiles should exhibit relatively low influence. Therefore, two different metrics can be derived for both lower fractiles and upper fractiles, which were named as *preservation metric* and *deletion metric*, combined named as perturbation metric. Formally, we define a

preservation metric and *deletion metric* for single fractile as

$$Q_{Preservation}(\phi, M, x) = \sum_{f \in \mathcal{F}} (\phi(x \otimes l_f(M) - \phi(x)) \tag{2}$$

$$Q_{Deletion}(\phi, M, x) = \sum_{f \in \mathcal{F}} (\phi(x \otimes u_f(M) - \phi(x)) \tag{3}$$

Here, $l_f(M)$ is the *lower* f-fractile of M, $u_f(M)$ is the *upper* f-fractile and $\mathcal{F}$ is the set of fractions $\{1/i \mid i = 0 \dots N\}$ where N is the number of features. Since $\phi(x)$ is a constant, it can be ignored during the computation. $Q_{Preservation}$ varies inversely with the average influence of the lower fractiles. It will be high if the category output decreases only slightly as we mask pixels from least to most salient. Similarly, $Q_{Deletion}$ is *low* if the category output decreases rapidly as pixels are masked from the most to least salient, implying high influence of *upper* fractiles. In sum, higher value of $Q_{Preservation}$ is preferred while lower value of $Q_{Deletion}$ is preferred.

3.2 Faithfulness Optimization

Fong *et al.* [7] introduced a new category of *perturbation methods* that uses gradient descent to optimize the attribution using a proxy for the perturbation metrics as the objective. This presents a challenge, as the fractiles are not differentiable functions of the attribution M. To address this, perturbation methods typically define a smoothed objective function in terms of a single perturbed image $\tilde{x}$. This perturbed image is a linear interpolation between the original image and the fully masked image R. That is, $\tilde{x} = M \odot x + (1 - M) \odot R$. The approximated preservation objective is to maximize $\phi(\tilde{x})$.

The objective mentioned above, while differentiable in terms of the attribution map M, presents a coarse approximation due to its consideration of only one perturbed image, as opposed to a sequence of N perturbed images. Moreover, it tends to have a trivial maximum at $M = 1$ which is clearly not faithful. To mitigate this issue, a regularization term is often introduced to impose an area constraint on the attribution map the M. For example, in [6], a ranking-based area loss is introduced that forces the non-zero part of the attribution to have a fixed area β. However, setting the hyperparameter β in a principled manner can be challenging. Lower area constraints often do not include sufficient information for adequate explanations, while higher values tend to produce noticeable artifacts.

To address this issue, we propose to approximate the perturbation metrics more accurately using a smooth approximation of the fractiles of M. This eliminates the need for the area hyperparameter. Consider optimizing the preservation metric, where our goal is to maximize the category output for the lower fractiles of M. For a given fraction f, we approximate the f-fractile by a mapping α_f from pixels to the interval $[0, 1]$. We chose not to employ a binary mapping because it is computationally expensive to optimize and often results in suboptimal solutions. We interpret $\alpha_f(p)$ as the probability that pixel p is *not* in the lower

f-fractile of M. The map must satisfy the constraint $\Sigma_p \alpha_f(p) = (1-f) \cdot N$, where N is the number of pixels.

For each fractile, we can approximate the expected values of the perturbed image as follows:

$$\tilde{x}_l(\alpha_f) = \alpha_f \odot x + (1-\alpha_f) \odot R \tag{4}$$

Where $\tilde{x}_l(f)$ is the perturbed images with lower f-fractile replaced. In the case where α_f is binary, this approximation is exact. We can minimize the influence of replaced lower fractiles f by maximizing $\phi(\tilde{x}_l)$ subject to the constraint $\Sigma_p \alpha[p] = (1-f) \cdot N$. In practice, we soften this constraint by including a loss term proportional to the area error. For each fractile, our loss function becomes:

$$l_p(\alpha_f) = -\phi(\tilde{x}_l(\alpha_f)) + \beta_1 \Delta \tag{5}$$

$$\Delta = |\Sigma_p \alpha_f(p) - (1-f) \cdot N| \tag{6}$$

where Δ is the area regulation term and β_1 is a hyperparameter which has minor effect on the optimization since we always expect the constraint to be satisfied. Now consider the entire sequence of fractiles $\{\alpha_f\}$ for f in $\mathcal{F}$. We say this sequence is *consistent* if $\alpha_a \leq \alpha_b$ for $a \geq b$. That is, if a pixel is in the lower 0.1-fractile, it must be in the lower 0.2-fractile, and so on. If the sequence of fractiles $\{\alpha_f\}$ is consistent and binary, we can reconstruct an attribution M from these fractiles by simply summing them as $M = \Sigma_{f \in \mathcal{F}} \alpha_f$. Similarly, the loss function for deletion metric can be computed as :

$$l_d(\alpha_f) = \phi(\tilde{x}_u(\alpha_f)) + \beta_1 \Delta \tag{7}$$

$$\tilde{x}_u(\alpha_f) = (1-\alpha_f) \odot x + \alpha_f \odot R \tag{8}$$

Implementation In practice, simultaneously optimizing all of the fractiles under these constraints is challenging. Instead, we choose a small set of fractions $f_1 \ldots f_k$ for efficiency. Meanwhile, for consistenct guarantee, we introduce a new variable δ_{f_i} and optimize for δ_{f_i} instead of α_{f_i} during the optimization process where $\delta_{f_i} = \alpha_{f_i} - \alpha_{f_{i-1}}$. We can then parameterize α_{f_i} as the cumulative sum of δ_{f_i}, where $\alpha_{f_k} = \sum_{i=1}^{k} \delta_{f_i}$. The values of δ_{f_i} are bounded to be non-negative to ensure consistency. After generating maps for different fractiles, The resulting saliency map is given by:

$$M = \Sigma_{i=1}^{k} \alpha_{f_i} \tag{9}$$

In effect, since the approximated fractiles α_{f_i} are smooth, the missing fractiles are obtained by interpolating between them. Since each $\delta_{\alpha_{f_i}}$ only account for a small fractiles change, we are also able to reduce the number of iterations during the optimization to save computation cost.

In experiment, we only optimize for preservation metric as it align better with internal faithfulness requirement as discussed in Sec. 3.3. We will refer to this optimization approach as the *ensemble method*. Experimentally, we find that

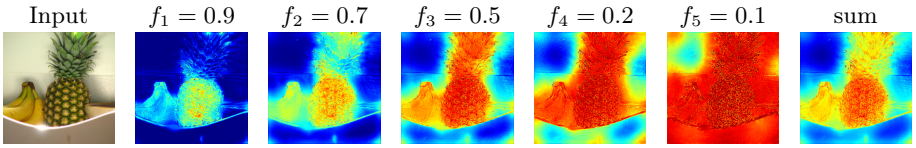

Fig. 1: attribution map generated by FEI_{IBM} for pineapple at different fractile

this approximation of the perturbation metrics demonstrate a better quantitative result, and that we can effectively optimize it by gradient descent. A visualization of the ensemble method is shown in Fig. 1.

3.3 Internal Faithfulness

Independently optimizing the fractiles of the attribution map offers the advantage of computational tractability. However, it also introduces a significant risk of over-optimization of the fractiles. While the intention is to interpret masking pixels as the elimination of information from the input image, it can inadvertently perturb the image in a way that activates feature recognizers in the hidden layer that are not directly relevant to the classification of the input image. This phenomenon, known as 'adversarial noise,' has been observed in prior work [8]. Various regularization methods have been proposed to address this challenge [5,6,30]. We contend that this problem arises due to a lack of faithfulness and can be mitigated through expanding the scope of faithfulness to hidden layer and the achieving *Internal Faithfulness*.

In the context of the perturbation-based optimization method, *Internal Faithfulness* implies that masking irrelevant features in the input should remove irrelevant features in the hidden layer and should not produce new feature encodings in the hidden layer. However, measuring this requires a solid understanding of how features are represented in the hidden layer. This is challenging due to the non-interpretable nature of the high-dimensional latent encoding in a neural network. Thus, it is imperative to identify a suitable proxy that effectively captures the model's underlying feature representation.

An intuitive proxy for internal faithfulness would be similarity of the hidden layer activation on the original and perturbed images. However, this would discourage removal of irrelevant features. Instead, we propose different methods and empirically test their performance to find the approximate proxies for feature representation. Our methods aim to match exact values, active values, inactive values, and binary status of the hidden layer activation. Moreover,since we attempt to match the feature representations relevant to the model decision, we should expect the perturbed input to produce the same result. Therefore, the preservation metric is required as objective function as shown in Eq. (5).

The matching can be achieved by adding a regulation term penalizing the difference of the perturbed internal activation and unperturbed one to the loss function. However, this approach is computationally and storage expensive, In-

stead, we choose gradient clipping, which cost-effective and does not introduce new gradients which may interfere with overall faithfulness goal.

To prevent the engagement of internal feature detectors that were not triggered in the unmasked image, Wagner *et al.* [30] proposed gradient clipping as an internal regulation method that clips gradient computations during optimization if the activation values fall outside a certain feasible range. However, their methods failed to identify proxies in the hidden layer and thus demonstrate sub-optimal performance as shown in Secs. 4.1 and 4.2. We adopt the idea of gradient clipping and tailor it towards different proxies.

Suppose h is a hidden layer of the network, and let x^h denote the activation of this layer on input x. Let ψ denote the category output as a function of layer x, such that $\phi(x) = \psi(x_h)$. Let γ_h denote the gradient of the category output with respect to layer h at the perturbed input value $\tilde{x}$, that is, $\gamma_h = \frac{\partial \psi(\tilde{x}^h)}{\partial \tilde{x}^h}$. We will define a clipped gradient $\tilde{\gamma}_h$. Intuitively, using the clipped gradient in optimization prevents the optimizer from reducing the loss by altering activations that are salient to the category output, and thus increases the internal faithfulness of the resulting attribution. This is done by setting the clipped gradient to zero in certain cases. By choosing when to clip, we explore how feature is encoded in the network.

First, we introduce gradient clipping by **V**alue **M**atching (**VM**) as follows:

$$\tilde{\gamma}_h = \begin{cases} 0 & \text{if } \gamma_h \geq 0 \wedge \tilde{x}^h > x^h \\ \gamma_h & \text{if } \gamma_h \geq 0 \wedge \tilde{x}^h \leq x^h \\ \gamma_h & \text{if } \gamma_h < 0 \wedge \tilde{x}^h > x^h \\ 0 & \text{if } \gamma_h < 0 \wedge \tilde{x}^h \leq x^h \end{cases} \tag{10}$$

This clipping mechanism aims to align with the exact values of the unperturbed hidden layer. When the activation with perturbed input exceeds that of the unperturbed one, we clip the positive gradient, preventing it from increasing further, implicitly causing it to decrease. Conversely, when the activation with masked input is lower than the unmasked one, we restrain the gradient that decreases the activation. This gradient clipping strategy matches the exact values of activation with the unperturbed input at the cost of clipping gradients beneficial for external faithfulness. To alleviate the strength of gradient clipping, we introduce two new gradient clipping methods which aim to match relatively active and inactive values by decomposing the VM method:

$$\tilde{\gamma_h} = \begin{cases} 0 & \text{if } \gamma_h \geq 0 \wedge \tilde{x}^h > x^h \\ \gamma_h & \text{Otherwise} \end{cases} \tag{11}$$

$$\tilde{\gamma_h} = \begin{cases} 0 & \text{if } \gamma_h < 0 \wedge \tilde{x}^h \leq x^h \\ \gamma_h & \text{Otherwise} \end{cases} \tag{12}$$

In Eq. (11), we encourage the reduction of overly activated neurons by clipping any gradient that attempts to increase their activation. In the case of asymmetric

activation function such as ReLU, this method encourages the inactivated part with unperturbed input to remain inactive, and as such, we term it **I**nactivated **V**alue **M**atching(**IVM**). Similarly, in Eq. (12), we encourage the activated part to remain active, which can be termed **A**ctivated **V**alue **M**atching(**AVM**). Furthermore, when asymmetric activation functions are involved, the gradient clipping condition can be further relaxed by using binary status as a proxy, leading to what we call **I**nactivated **B**inary **M**atching (**IBM**).

$$\tilde{\gamma_h} = \begin{cases} 0 & \text{if } \gamma_h \geq 0 \wedge x^h \leq 0 \\ \gamma_h & \text{Otherwise} \end{cases} \tag{13}$$

In this case, our objective is to match the binary status of x^h. Eq. (13) is obtained by by introducing a condition $x^h \leq 0$ to Eq. (11). This condition ensures that we only clip the gradient for the original inactivated neurons while disregarding the value of the activated ones. Similarly, a condition of $x^h \geq 0$ can be added to Eq. (12), but it doesn't alter the clipping condition.

The four different gradient clipping methods achieve certain level of internal faithfulness while maintaining overall faithfulness. The differences in their performance is shown in Secs. 4.1 and 4.2. In practical implementation, we apply gradient clipping only to feature extraction layers, considering this part of model identify features for decision-making. We call the combination of the ensemble attribution method with gradient clipping **F**aithfulness-guided **E**nsemble **I**nterpretation, referred to as FEI. The variations of this method using our four gradient clipping approaches are denoted FEI_{VM}, FEI_{IVM}, FEI_{AVM}, and FEI_{IBM}, each tailored to specific faithfulness considerations.

4 Evaluation

We now apply the method to obtain insight into the functioning of CNN's on image recognition tasks. All evaluation metric use the ImageNet validation dataset [19]. A reference image with random monotone color is used in each optimization iteration and the ensemble of fraction $f_k \in [0.1, 0.3, 0.5, 0.7, 0.9]$ are applied. The map α_{f_k} for each fractile f_k is optimized for 100 iterations with $\beta_1 = i \cdot e^{-2}$ which increases with the iteration number i. Each map is optimized with Adam optimizer [14]. The methods we are comparing against includes **E**xtremal **P**erturbation(EP) [6], RISE [17], FGVis [30], and GradCam [21].

4.1 Visualization

A qualitative visualization comparison among different perturbation-based methods is presented in Fig. 2. We only present visualizations from this group of methods as they tend to produce the best quality of visualization. Hot areas with red color are considered important for model decision whether cold area with blue color are less relevant. In comparison to coarse attribution maps such as EP and RISE, our method demonstrates a more precise identification of the

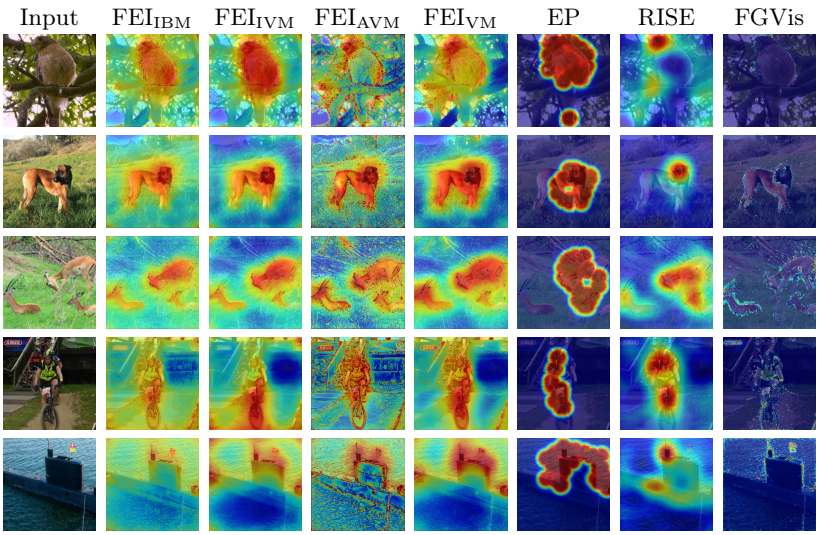

Fig. 2: We compared our method with to other perturbation methods. Results generated from its official implementation and our re-implementation. The attribution are generated for VGG16 network [24]. The object in top down order are *Bald Eagle*, *Boxer*, *Impala*, *Mountain bike*, and *Submarine*

subject.EP may also identify some objects but it provide a very coarse selection as the shape of its attribution is restricted. RISE produce a similar heatmap as our method but sometimes is only able to locate part of the subject. In contrast to FGVis, our visualization conveys more information about the overall image, as opposed to merely displaying isolated edge maps. Among different variation of FEI, FEI$_{\text{AVM}}$ seems to produce more noisy maps with edges. The clipping method of FEI$_{\text{AVM}}$ allows originally inactivated neuron to be activated, which might be source of noise. Meanwhile, all other three methods do a better job in locating objects than other methods. In general, our approach provides subjectively superior visualizations in terms of identifying relevant image regions without extraneous artifacts.

4.2 Perturbation Result

Tab. 1 presents the preservation and deletion scores, comparing our method with prior methods. Each method is evaluated using 1000 images, and results for stochastic methods are reported as an average of three measurements. We plot the softmax score of the desired category against the area threshold and compute the AUC for both metrics. Higher values are better for preservation, while lower values are better for deletion. FEI$_{\text{IBM}}$ achieves the best score in the preservation metric. Though FGVis performs slightly better in deletion score for VGG16, FEI$_{\text{IBM}}$ and FEI$_{\text{AVM}}$ both have comparable performance. Moreover, all variations of FEI perform better than FGVis with both metrics in ResNet34.

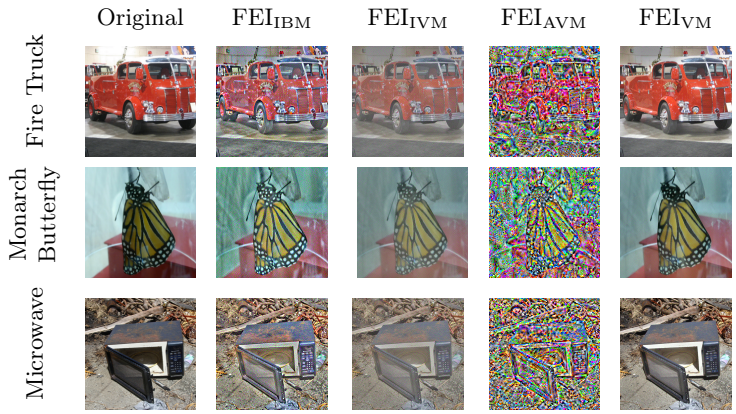

Fig. 3: Image reconstruction from gradient clipping. The model we use is VGG16

Among our ensemble methods, FEI$_{\text{IBM}}$ exhibits the best overall performance, which is consistent with its most relaxed gradient clipping criterion from Eq. (5).

Ablation Study In our ablation study, we aimed to assess the effectiveness of ensemble method as well as internal faithfulness clipping method with FEI$_{\text{IBM}}$ as the baseline. We implemented several variations for comparison: FEI$_{\text{no-clipping}}$: This implementation employed the ensemble method without the gradient clipping regulation; IBM$_{\text{no ensemble}}$: In this variant, we omit Δ from Eq. (5) and only generate one attribution map; IBM$_{L_1}$: we only generate one map with $f = 1$, making Δ equivalent to a L_1 regulation. All three variants shows inferior result in preservation scores. Though IBM$_{\text{no ensemble}}$ desmonstrates a slightly better deletion score for VGG16, it has a much worse preservation score. This suggests the superiority of both ensemble methods and internal faithful gradient clipping.

4.3 Image Reconstruction

We propose an image reconstruction metric to evaluate the effectiveness of internal faithfulness. The intuition is that similar internal representations during inference should imply a similar input. We attempt to regenerate an image from scratch using gradient descent with gradient clipping methods and the pretrained model. Using the loss function $l_{rec}(x)$ where $l_{rec}(x) = -\phi(x)$, we initialize x with noise and employ various gradient clipping techniques to optimize x with respect to $l_{rec}(x)$. The results are shown in Fig. 3. The optimized input are clipped to be within the feasible range of images. Surprisingly, gradient clipping techniques alone are sufficient to recover the image to a strong extent. We can see that FEI$_{\text{VM}}$ produces a reconstruction with the best quality, while FEI$_{\text{IBM}}$ and FEI$_{\text{IVM}}$ both produce comparable results. FEI$_{\text{AVM}}$ shows noisy images, which demonstrate FEI$_{\text{AVM}}$ may use an inappropriate proxy for feature representation.

Table 1: Quantitative Faithfullness evaluation of perturbation method with Gaussian-blurred image as reference for preservation and Grey image as reference for deletion on VGG16 [24] and ResNet34 [9], Implementation from RISE [17]

Method	VGG16		ResNet34	
	Preservation	Deletion	Preservation	Deletion
GradCam	0.624	0.128	0.648	0.138
RISE	0.620±0.014	0.118±0.0048	0.642±0.007	0.129±0.005
Extremal Perturbation	0.461±0.010	0.236±0.001	0.520±0.008	0.234±0.009
FGVis	0.400±0.011	**0.060**±0.001	0.469±0.005	0.132±0.006
FEI_{IBM}	**0.656**±0.004	0.080±0.004	**0.732**±0.006	0.121±0.004
FEI_{IVM}	0.583±0.008	0.127±0.006	0.635±0.008	**0.096**±0.004
FEI_{AVM}	0.622±0.004	0.080±0.003	0.658±0.009	0.108±0.002
FEI_{VM}	0.601±0.006	0.114±0.004	0.627±0.017	0.096±0.003
$\text{FEI}_{\text{no-clipping}}$	0.511 ±0.003	0.194±0.004	0.546±0.005	0.272±0.005
$\text{IBM}_{\text{no ensemble}}$	0.458 ±0.001	0.075±0.003	0.649±0.002	0.136±0.004
IBM_{L_1}	0.420 ±0.008	0.270±0.001	0.481 ±0.009	0.275±0.003

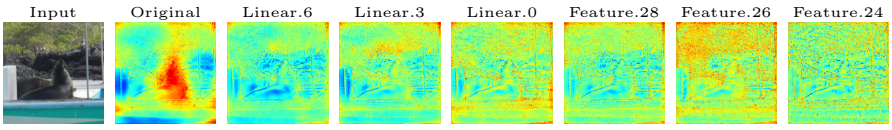

Fig. 4: Sanity Check for *Sea Lion* with VGG16 and FEI_{IBM}

4.4 Defense Evaluation

The proposed gradient clipping methods help the explanation achieve internal faithfulness during optimization. As a result, they also enhance the defense against adversarial noise, which is common in perturbation-based methods. We conducted a quantitative evaluation of the defense effects of our methods, as summarized in Tab. 2. We tested the frequency of successfully generating an attribution map for a black image across all targets, following the experimental setup of *FGVis* [30], with which we compare our results. Our gradient clipping methods show outstanding ability in preventing adversarial attributions, with the exception of FEI_{AVM} on AlexNet and VGG16. Its inferior results may be due to the fact that it is matching the activated unit instead of the inactivated unit, which potentially activate originally inactivated neurons.

4.5 Sanity Check

The sanity check proposed by Adebayo *et al.* [1] is used to examine the change in attribution when model weights are randomized. We adopted the cascading random setup and visualized the attribution maps generated for the randomized model, as shown in Fig. 4. Upon randomizing a single layer of weights,

Table 2: How often an explanation is generated for a black image. Results are generated on Alexnet [15],ResNet50 [9],VGG16 [24] and GoogLeNet [29]

Model	Defense mechanism					
	FGiVs	FEI_{IBM}	FEI_{IVM}	FEI_{AVM}	FEI_{VM}	No Clipping
Alexnet	0.2%	4.2%	1.3%	95.7%	0.4%	100%
ResNet50	0.2%	0.1%	0%	0%	0.1%	100%
VGG16	0%	0.1%	0.1%	96.0%	0.1%	100%
GoogLeNet	0.1%	0.3%	0%	0.1%	0%	100%

the generated explanation loses focus on the object and introduces considerable noise. As the model undergoes cascading randomization, more noise is generated. However, we can observe an edge map preserved in the attribution map. This is because the internal faithfulness regulation encourages faithfulness in the unrandomized earlier layers, which appears to contribute to edge detection.

5 Ethical Statement

Our work potentially aids in attacks that can fool neural network predictions. However, we believe that overall neural network explanations will help identify bias in neural networks and better serve society. In future research, we will also replace the original ImageNet dataset [19] with the face-obscured version [31].

6 Conclusion and Future work

We have introduced **F**aithfulness-guided **E**nsemble **I**nterpretation(FEI), a novel neural network explanation method that enhances both the breadth and effectiveness of faithfulness for the model. Our approach combines ensemble approximation, inspired by quantitative faithfulness metrics, with gradient clipping, inspired by internal activation matching. Additionally, we have proposed a new qualitative metric that implicitly assesses internal faithfulness. Our empirical results shows that activating originally inactivated neurons during perturbation may produce irrelevant noises and artifacts in input, which suggest features might be represented in the activated part of hidden layers. Overall, FEI has demonstrated superior results in both qualitative visualization and quantitative evaluation. Although we can generate faithful attribution maps for model decisions, the internal process remains uninterpretable. In the future, we plan to elucidate the explanation of the intermediate process of model inference. Our future goal is to interpret the internal structure of the model and enhance our method based on it.

References

1. Adebayo, J., Gilmer, J., Muelly, M., Goodfellow, I., Hardt, M., Kim, B.: Sanity checks for saliency maps. Advances in neural information processing systems **31** (2018) 3, 4, 13
2. Bach, S., Binder, A., Montavon, G., Klauschen, F., Müller, K.R., Samek, W.: On pixel-wise explanations for non-linear classifier decisions by layer-wise relevance propagation. PloS one **10**(7), e0130140 (2015) 3
3. Binder, A., Montavon, G., Lapuschkin, S., Müller, K.R., Samek, W.: Layer-wise relevance propagation for neural networks with local renormalization layers. In: Artificial Neural Networks and Machine Learning–ICANN 2016: 25th International Conference on Artificial Neural Networks, Barcelona, Spain, September 6-9, 2016, Proceedings, Part II 25. pp. 63–71. Springer (2016) 4, 5
4. Chattopadhay, A., Sarkar, A., Howlader, P., Balasubramanian, V.N.: Grad-cam++: Generalized gradient-based visual explanations for deep convolutional networks. In: 2018 IEEE winter conference on applications of computer vision (WACV). pp. 839–847. IEEE (2018) 1, 3
5. Du, M., Liu, N., Song, Q., Hu, X.: Towards explanation of dnn-based prediction with guided feature inversion. In: Proceedings of the 24th ACM SIGKDD International Conference on Knowledge Discovery & Data Mining. pp. 1358–1367 (2018) 8
6. Fong, R., Patrick, M., Vedaldi, A.: Understanding deep networks via extremal perturbations and smooth masks. In: Proceedings of the IEEE/CVF international conference on computer vision. pp. 2950–2958 (2019) 3, 6, 8, 10
7. Fong, R.C., Vedaldi, A.: Interpretable explanations of black boxes by meaningful perturbation. In: Proceedings of the IEEE international conference on computer vision. pp. 3429–3437 (2017) 2, 3, 6
8. Ghorbani, A., Abid, A., Zou, J.: Interpretation of neural networks is fragile. In: Proceedings of the AAAI conference on artificial intelligence. vol. 33, pp. 3681–3688 (2019) 8
9. He, K., Zhang, X., Ren, S., Sun, J.: Deep residual learning for image recognition. In: Proceedings of the IEEE conference on computer vision and pattern recognition. pp. 770–778 (2016) 13, 14
10. Hinton, G., Vinyals, O., Dean, J., et al.: Distilling the knowledge in a neural network. arXiv preprint arXiv:1503.02531 **2**(7) (2015) 3
11. Hooker, S., Erhan, D., Kindermans, P.J., Kim, B.: A benchmark for interpretability methods in deep neural networks. Advances in neural information processing systems **32** (2019) 4
12. Jacovi, A., Goldberg, Y.: Towards faithfully interpretable nlp systems: How should we define and evaluate faithfulness? arXiv preprint arXiv:2004.03685 (2020) 1
13. Kapishnikov, A., Bolukbasi, T., Viégas, F., Terry, M.: Xrai: Better attributions through regions. In: Proceedings of the IEEE/CVF International Conference on Computer Vision. pp. 4948–4957 (2019) 4
14. Kingma, D.P., Ba, J.: Adam: A method for stochastic optimization. arXiv preprint arXiv:1412.6980 (2014) 10
15. Krizhevsky, A., Sutskever, I., Hinton, G.E.: Imagenet classification with deep convolutional neural networks. Advances in neural information processing systems **25** (2012) 14
16. Lundberg, S.M., Lee, S.I.: A unified approach to interpreting model predictions. Advances in neural information processing systems **30** (2017) 4

17. Petsiuk, V., Das, A., Saenko, K.: Rise: Randomized input sampling for explanation of black-box models. arXiv preprint arXiv:1806.07421 (2018) 3, 10, 13
18. Ribeiro, M.T., Singh, S., Guestrin, C.: " why should i trust you?" explaining the predictions of any classifier. In: Proceedings of the 22nd ACM SIGKDD international conference on knowledge discovery and data mining. pp. 1135–1144 (2016) 1, 3, 4, 5
19. Russakovsky, O., Deng, J., Su, H., Krause, J., Satheesh, S., Ma, S., Huang, Z., Karpathy, A., Khosla, A., Bernstein, M., Berg, A.C., Fei-Fei, L.: ImageNet Large Scale Visual Recognition Challenge. International Journal of Computer Vision (IJCV) **115**(3), 211–252 (2015). https://doi.org/10.1007/s11263-015-0816-y 10, 14
20. Samek, W., Binder, A., Montavon, G., Lapuschkin, S., Müller, K.R.: Evaluating the visualization of what a deep neural network has learned. IEEE transactions on neural networks and learning systems **28**(11), 2660–2673 (2016) 4
21. Selvaraju, R.R., Cogswell, M., Das, A., Vedantam, R., Parikh, D., Batra, D.: Grad-cam: Visual explanations from deep networks via gradient-based localization. In: Proceedings of the IEEE international conference on computer vision. pp. 618–626 (2017) 1, 3, 10
22. Shrikumar, A., Greenside, P., Kundaje, A.: Learning important features through propagating activation differences. In: International conference on machine learning. pp. 3145–3153. PMLR (2017) 3
23. Simonyan, K., Vedaldi, A., Zisserman, A.: Deep inside convolutional networks: Visualising image classification models and saliency maps. arXiv preprint arXiv:1312.6034 (2013) 3
24. Simonyan, K., Zisserman, A.: Very deep convolutional networks for large-scale image recognition. arXiv preprint arXiv:1409.1556 (2014) 11, 13, 14
25. Smilkov, D., Thorat, N., Kim, B., Viégas, F., Wattenberg, M.: Smoothgrad: removing noise by adding noise. arXiv preprint arXiv:1706.03825 (2017) 1, 3
26. Springenberg, J.T., Dosovitskiy, A., Brox, T., Riedmiller, M.: Striving for simplicity: The all convolutional net. arXiv preprint arXiv:1412.6806 (2014) 3
27. Sun, Y., Chockler, H., Huang, X., Kroening, D.: Explaining image classifiers using statistical fault localization. In: European Conference on Computer Vision. pp. 391–406. Springer (2020) 3
28. Sundararajan, M., Taly, A., Yan, Q.: Axiomatic attribution for deep networks. In: International conference on machine learning. pp. 3319–3328. PMLR (2017) 1, 3
29. Szegedy, C., Liu, W., Jia, Y., Sermanet, P., Reed, S., Anguelov, D., Erhan, D., Vanhoucke, V., Rabinovich, A.: Going deeper with convolutions. In: Proceedings of the IEEE conference on computer vision and pattern recognition. pp. 1–9 (2015) 14
30. Wagner, J., Kohler, J.M., Gindele, T., Hetzel, L., Wiedemer, J.T., Behnke, S.: Interpretable and fine-grained visual explanations for convolutional neural networks. In: Proceedings of the IEEE/CVF Conference on Computer Vision and Pattern Recognition. pp. 9097–9107 (2019) 2, 3, 8, 9, 10, 13
31. Yang, K., Yau, J., Fei-Fei, L., Deng, J., Russakovsky, O.: A study of face obfuscation in imagenet. arXiv preprint arXiv:2103.06191 (2021) 14
32. Zeiler, M.D., Fergus, R.: Visualizing and understanding convolutional networks. In: European conference on computer vision. pp. 818–833. Springer (2014) 3
33. Zhang, J., Bargal, S.A., Lin, Z., Brandt, J., Shen, X., Sclaroff, S.: Top-down neural attention by excitation backprop. International Journal of Computer Vision **126**(10), 1084–1102 (2018) 4

34. Zhou, B., Khosla, A., Lapedriza, A., Oliva, A., Torralba, A.: Learning deep features for discriminative localization. In: Proceedings of the IEEE conference on computer vision and pattern recognition. pp. 2921–2929 (2016) 3